In Vivo Molecular Imaging of Atherosclerotic Lesions in ApoE$^{-/-}$ Mice Using VCAM-1–Specific, ^{99m}Tc-Labeled Peptidic Sequences

Julien Dimastromatteo[1,2], Alexis Broisat[1,2], Pascale Perret[1,2], Mitra Ahmadi[1,2], Didier Boturyn[2,3], Pascal Dumy[2,3], Daniel Fagret[1,2], Laurent M. Riou[1,2], and Catherine Ghezzi[1,2]

[1]INSERM, U1039, Radiopharmaceutiques Biocliniques, Grenoble, France; [2]UJF-Grenoble 1, Grenoble, France; and [3]Département de Chimie Moléculaire, UMR CNRS-UJF 5250, Grenoble, France

Vascular cell adhesion molecule 1 (VCAM-1) plays a major role in the chronic inflammatory processes involved in vulnerable atherosclerotic plaque development. We previously showed that the ^{99m}Tc-labeled major histocompatibility complex 1–derived peptide B2702p bound specifically to VCAM-1 and allowed the ex vivo imaging of atherosclerotic lesions in Watanabe heritable hyperlipidemic rabbits. However, B2702p target-to-background ratio was suboptimal for the in vivo imaging of VCAM-1 expression in atherosclerotic lesions. To improve the target-to-background ratio, 20 derivatives of B2702p (B2702p1–B2702p20) were synthesized using the alanine scan methodology. We hypothesized that ^{99m}Tc-radiolabeled B2702p derivatives might allow the molecular imaging of VCAM-1 expression in an experimental model of atherosclerosis. **Methods:** A mouse model of focal atherosclerotic plaque development induced by left carotid artery ligation in apolipoprotein E double-knockout (ApoE$^{-/-}$) mice was used (n = 82). ^{99m}Tc-B2702p and ^{99m}Tc-B2702p1–^{99m}Tc-B2702p20 were injected intravenously in anesthetized animals 3 wk after the ligation. Whole-body planar imaging was performed for 3 h. SPECT imaging of 6 additional ligated ApoE$^{-/-}$ mice was also performed with ^{99m}Tc-B2702p1. The animals were then euthanized, and the biodistribution of ^{99m}Tc-labeled peptides was evaluated by γ-well counting of excised organs. Expression of VCAM-1 in the ligated and contralateral carotid arteries was evaluated by immunohistology. **Results:** Robust VCAM-1 immunostaining was observed in the left carotid atherosclerotic lesions as a consequence of artery ligation, whereas no VCAM-1 expression was detected in the contralateral carotid artery. Among all evaluated peptides, ^{99m}Tc-B2702p1 exhibited the most favorable properties. By γ-well counting, there was a significant 2.0-fold increase in the ^{99m}Tc-B2702p1 left-to-right carotid artery activity ratio (2.6 ± 0.6) and a 3.4-fold increase in the left carotid-to-blood activity ratio (1.4 ± 0.4) in comparison to ^{99m}Tc-B2702p (1.3 ± 0.2 and 0.4 ± 0.1, respectively, $P < 0.05$ for both comparisons). Similarly, planar image quantification indicated a higher left-to-right carotid activity ratio in ^{99m}Tc-B2702p1– than in ^{99m}Tc-B2702p–injected mice (1.2 ± 0.1 vs. 1.0 ± 0.0, respectively, $P < 0.05$). Finally, a significantly higher ^{99m}Tc-B2702p1 activity in the left than in the right carotid artery was observed by SPECT imaging (2.2 ± 0.4 vs. 1.4 ± 0.3 cpm/mm^2/injected dose, respectively, $P < 0.05$). **Conclusion:** ^{99m}Tc-B2702p1 is a potentially useful radiotracer for the in vivo molecular imaging of VCAM-1 expression in atherosclerotic plaques.

Received Oct. 15, 2012; revision accepted Feb. 11, 2013.
For correspondence or reprints contact: Laurent M. Riou, Faculté de Médecine, Bâtiment Jean Roget, 38700 La Tronche, France.
E-mail: laurent.riou@ujf-grenoble.fr
Published online May 29, 2013.

Key Words: VCAM-1; molecular imaging; vulnerable atherosclerotic plaque

J Nucl Med 2013; 54:1442–1449
DOI: 10.2967/jnumed.112.115675

Cardiovascular diseases represent the primary cause of mortality worldwide (*1*), mostly because there is an unmet need for an efficient screening prevention strategy as illustrated by the fact that sudden cardiac death and acute myocardial infarction are the first symptoms of atherosclerosis in more than 50% of cardiovascular disease patients (*2*). A noninvasive test allowing the detection of coronary vulnerable atherosclerotic lesions in asymptomatic patients before the occurrence of a cardiovascular event would therefore greatly participate in the overall effort at decreasing the burden of cardiovascular diseases (*1–4*). Nuclear molecular imaging would be perfectly suited for this purpose because of the functional nature of the information provided by this noninvasive imaging methodology (*5*). Several molecular targets have been evaluated for the development of corresponding specific radiolabeled imaging agents (*6*). Among other relevant molecules, vascular cell adhesion molecule 1 (VCAM-1) is a well-recognized marker of atherosclerotic plaque vulnerability (*3,4,7–9*) since its overexpression is observed over the complete course of vulnerable plaque development (*10,11*). In addition, overexpression of VCAM-1 is strictly restricted to areas of plaque development (*7*), and several cell types participating in the evolution of a given atherosclerotic lesion toward a vulnerable plaque overexpress VCAM-1, namely luminal endothelial cells (*12*), macrophages (*13*), smooth muscle cells (*14*), and intraplaque neovessels (*10*). We have previously investigated the possibility of imaging VCAM-1 expression in a Watanabe heritable hyperlipidemic rabbit model of atherosclerosis using ^{99m}Tc- and ^{123}I-labeled versions of the VCAM-1–specific major histocompatibility complex 1–derived peptide B2702p (*15,16*). Despite specific binding to aortic atherosclerotic lesions overexpressing VCAM-1 after in vivo injection and ex vivo autoradiographic imaging, the significant circulating blood activity of ^{99m}Tc- and ^{123}I-B2702p prevented in vivo image acquisition. Discrete modifications in the amino acid sequence of a peptide might allow improvements in the in vivo biodistribution properties of the molecule without affecting its binding specificity (*17–19*). We therefore generated 20 derivatives of the previously evaluated B2702p peptide to test the hypothesis

that limited modifications to the B2702p sequence might improve the blood elimination kinetics of the tracer while retaining VCAM-1–specific binding properties suitable for the in vivo imaging of VCAM-1 expression in an apolipoprotein E double-knockout ($ApoE^{-/-}$) mouse model of atherosclerosis.

MATERIALS AND METHODS

Peptide Synthesis and Radiolabeling

The peptidic sequences of B2702p1–B2702p20 are presented in Table 1. All derivatives were synthesized by Eurogentec France SASU. The sequence of ^{99m}Tc-B2702p1 mismatch is a random version of that of ^{99m}Tc-B2702p1. The systematic presence of a histidine residue at the N terminal end of all derivatives allowed ^{99m}Tc radiolabeling with [$^{99m}Tc(OH_2)_{(3)}$ $(CO)_{(3)}$] using a tridentate ligand system. The precursor [$^{99m}Tc(OH_2)_{(3)}$ $(CO)_{(3)}$] was synthesized using a tricarbonyl pharmaceuticals kit (Isolink; Mallinckrodt). The kit was reconstituted with 2 GBq of $^{99m}TcO_4^-$ (Schering SA) and incubated at 100°C for 20 min before pH adjustment to 8.0 using HCl 2N.

A 1,100- to 1,500-MBq quantity of the reconstituted kit was added to 32 nmol (50 μg) of B2702p1–B2702p20 and incubated for 20 min at 80°C. The radiochemical purity was determined using high-performance liquid chromatography on a Licrosorb RP-C18 column (Supelco) (5 μm, 4.6 × 250 mm). The solvent system consisted of H_2O–0.1% trifluoroacetic acid (solvent A) and 90% acetonitrile–0.1% trifluoroacetic acid (solvent B) with a flow rate of 1 mL/min. Tracer was eluted by applying a gradient of 5% B during 5 min, a linear gradient from 5% to 60% during 15 min, and 60% B during 5 min before the system returned to the initial conditions within 5 min.

In Vitro Fluorescence Polarization Experiments

Binding of B2702p1 to VCAM-1 was evaluated in vitro by fluorescence polarization using a fluorescent analog of B2702p1 ([F]-B2702-p1). The fluorescence polarization of a 12.5 nM (100 μL) solution of [F]-B2702p1 was measured in the absence of VCAM-1 or after incremental additions (0.5 μL) of a 13.5 μM solution of the adhesion molecule using a Perkin-Elmer LS 50 spectrometer. Control experiments were conducted by replacing VCAM-1 by bovine serum albumin as a nonspecific ligand (final concentration ranging from 0 to 27 μmol/L). The experiments were performed in triplicate. Anisotropy data (*A,* arbitrary units) were fitted using the formula $A = A_0 + (A_{max} - A_0) \times ([target]/(K_d + [target]))$ for a one-to-one interaction where A_0 represents the anisotropy value in the absence of VCAM-1 and A_{max} the maximum anisotropy value that was observed in the presence of increasing concentrations of the molecular target (VCAM-1 or bovine serum albumin) (*20*). The K_d value for the interaction between [F]-B2702p1 and VCAM-1 or bovine serum albumin was determined according to this equation.

Experimental Protocol

Experimental Model. All experiments were approved by the Animal Care and Use Committee of the Military Research and Health Center (CRSSA, authorization no. 2006/37.0), Grenoble, France. All experiments were performed under the supervision of an authorized individual (authorization no. 38 05 39). Eighty-two hypercholesterolemic female $ApoE^{-/-}$ mice weighing 19.3 ± 0.2 g were obtained from Charles River Laboratories. The animals were anesthetized using an intraperitoneal injection of one-third xylazine (10 mg/kg) and two-thirds ketamine (100 mg/kg). The skin was incised at the level of the thyroid gland, and the left common carotid artery was ligated near the bifurcation using 5-0 silk (Ethicon). The incision was then sutured, and the animals were allowed to return to individual cages.

In Vivo Imaging and Biodistribution Studies. Three weeks after left carotid artery ligation, the animals were reanesthetized and 34.7 ± 0.8 MBq of tracer were injected through a tail vein. The animals were then placed on the parallel-hole collimator of a small-animal

TABLE 1
Peptidic Sequence, Radiochemical Purity, and Urinary Stability of ^{99m}Tc-B2702p1-20 Peptides

Tracer	Peptidic sequence	RCP (%)	Stability (%)
^{99m}Tc-B2702p	H_2N-HGR ENL RIA LRY-COOH	90	93
^{99m}Tc-B2702p1	H_2N-HGR ANL RIL ARY-COOH	92	94
^{99m}Tc-B2702p1 mismatch	H2N- HGL RAY IRA RNL-COOH	90	89
^{99m}Tc-B2702p2	H_2N-HGR ENL AIL ARY-COOH	95	96
^{99m}Tc-B2702p3	H_2N-HGR ENL RIL ARA-COOH	97	83
^{99m}Tc-B2702p4	H_2N-HGR ENL RIL AAY-COOH	95	92
^{99m}Tc-B2702p5	H_2N-HGR ENL RIL ARY-COOH	50	N/D
^{99m}Tc-B2702p6	H_2N-HGR ENA RIL ARY-COOH	93	95
^{99m}Tc-B2702p7	H_2N-HGA ENL RIL ARY-COOH	95	50
^{99m}Tc-B2702p8	H_2N-HGR ENL RIA ARY-COOH	80	84
^{99m}Tc-B2702p9	H_2N-HGR EAL RIL ARY-COOH	95	97
^{99m}Tc-B2702p10	H_2N-HGR ENL RIL ARY-COOH	95	99
^{99m}Tc-B2702p11	H_2N-HGA ENL RIA LRY-COOH	97	82
^{99m}Tc-B2702p12	H_2N-HGR ANL RIA LRY-COOH	88	80
^{99m}Tc-B2702p13	H_2N-HGR EAL RIA LRY-COOH	96	79
^{99m}Tc-B2702p14	H_2N-HGR ENA RIA LRY-COOH	96	76
^{99m}Tc-B2702p15	H_2N-HGR ENL AIA LRY-COOH	96	85
^{99m}Tc-B2702p16	H_2N-HGR ENL RAA LRY-COOH	91	70
^{99m}Tc-B2702p17	H_2N-HGR ENL RIA LAY-COOH	90	80
^{99m}Tc-B2702p18	H_2N-HGR ENL RIA LRA-COOH	88	81
^{99m}Tc-B2702p19	H_2N-HGR ANL RIL ARA-COOH	88	79
^{99m}Tc-B2702p20	H_2N-HGR ANL RIL AAY-COOH	92	78

N/D = not determined; RCP = radiochemical purity.

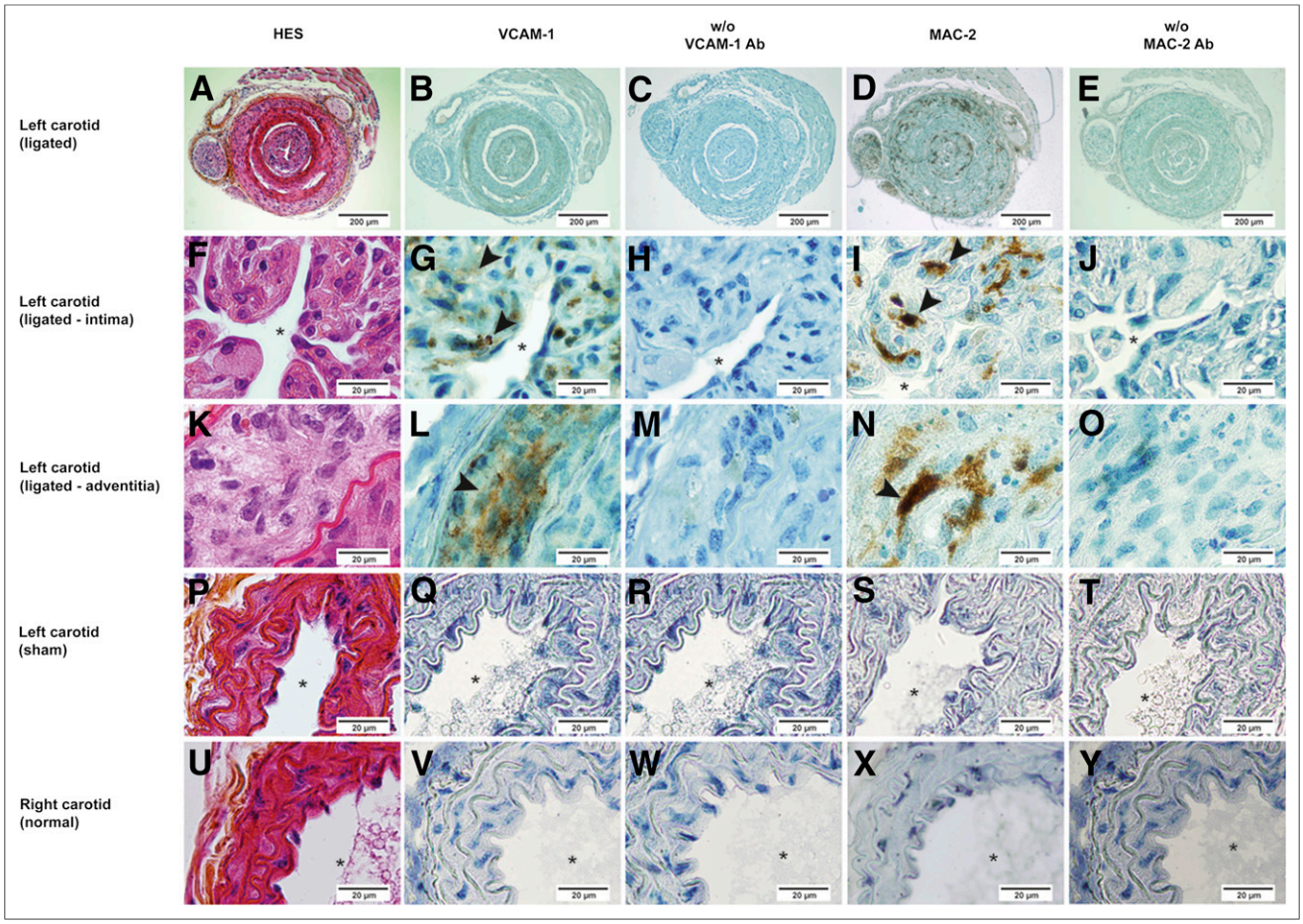

FIGURE 1. Histologic (hematoxylin, erythrosine, and safran) and immunohistologic staining of VCAM-1 and Mac-2 expression in ApoE$^{-/-}$ mouse carotid vessels. Histochemistry and immunohistochemistry were performed on adjacent transverse sections of atherosclerotic lesions from ligated left carotid arteries (A–E), with magnifications centered on intimal and adventitial areas (F–J and K–O, respectively) and on nonligated left carotid arteries from sham-operated ApoE$^{-/-}$ animals (P–T) and on contralateral, right, carotid arteries (U–Y). Positive VCAM-1 and Mac-2 immunostaining was observed in atherosclerotic lesions developing at site of left carotid artery ligation but not in vessels from sham-operated animals and right carotid arteries. Specificity of immunostaining was assessed by performing control experiments in absence of VCAM-1– and Mac-2–specific primary antibodies (without VCAM-1 Ab and without MAC-2 Ab). Ab = antibody; HES = hematoxylin, erythrosine, and safran; w/o = without.*Vessel lumen.

dedicated γ-camera (γ-Imager; Biospace Lab), and planar imaging was performed for 180 min in the list mode using a 125- to 150-keV energy window with anesthesia being maintained using isoflurane, 1%. High-resolution, pinhole SPECT imaging of ^{99m}Tc-B2702p1 and ^{99m}Tc-B2702p was also performed 150 and 210 min after tracer injection using the same imaging system (n = 6 and 4, respectively).

Regions of interest were drawn on the left carotid lesional area and on the contralateral vessel on both planar and tomographic images, and tracer activity was expressed as cpm/mm^2/MBq. Images were reconstructed using γ-acquisition software and an ordered-subsets expectation maximization algorithm. At the end of image acquisition, the animals were euthanized by an overdose of intraperitoneally administered pentobarbital, and samples from the left and right carotid arteries, aorta, lung, liver, spleen, blood, adipose tissue, and skeletal muscle were obtained together with the heart, kidney, and thyroid. The blood kinetics of ^{99m}Tc-B2702p1 were also determined after intravenous injection, and euthanasia followed by blood withdrawal and left and right carotid excision at 15 (n = 3) and 60 min (n = 3) after injection. The tissue samples and organs were quickly rinsed and weighed, and their activities were assessed using a γ-well counter (Cobra II; Packard Instruments) and a 100- to 168-keV energy window. Tracer activity was expressed as percentage injected dose per gram of wet weight. Urine and blood were also sampled to assess the stability of the injected tracers using high-performance liquid chromatography as described for the radiochemical purity determination.

Histology and Immunohistology. Standard trichrome staining (hematoxylin, erythrosine, and safran) for nuclei, cytoplasm, and fibrosis staining, and immunohistologic staining of VCAM-1 and Mac-2, were performed using previously described procedures (*21*).

Statistical Analysis

Values are presented as mean ± SD. Statistical computations were performed using SYSTAT software (SPSS, Inc.). Between-groups comparisons were performed using the unpaired t test and Kruskal–Wallis test, whereas within-group analysis was performed using 1-way ANOVA and the Wilcoxon signed-rank test. P values of 0.05 or less were considered statistically significant.

RESULTS

Histology and Immunohistology

As shown in Figure 1, left carotid artery ligation resulted in atherosclerotic lesion development at the site of occlusion. Posi-

TABLE 2
Biodistribution of ^{99m}Tc-B2702p1-20 at 180 Minutes After Injection in ApoE$^{-/-}$ Mice with Left Carotid Artery Ligation

Tracer	Heart	Aorta	Lung	Liver	Spleen	Kidney	Fat	Muscle	Blood	Thyroid	L. carotid	R. carotid
^{99m}Tc-B2702p	1.5 ± 0.1	2.7 ± 0.4	3.9 ± 0.4	10.6 ± 2.6	2.2 ± 0.3	69.0 ± 13.0	1.0 ± 0.2	1.2 ± 0.2	5.7 ± 0.6	9.7 ± 3.0	2.4 ± 0.4	1.8 ± 0.3
^{99m}Tc-B2702p1	0.3 ± 0.1	0.5 ± 0.1	0.8 ± 0.1	3.1 ± 0.6	1.6 ± 0.7	4.6 ± 0.5	0.2 ± 0.0	0.1 ± 0.0	0.9 ± 0.2†	0.7 ± 0.2	1.3 ± 0.4*	0.5 ± 0.1†
^{99m}Tc-B2702p1 mismatch	0.7 ± 0.2	1.7 ± 0.7	1.7 ± 0.4	22.1 ± 5.9	0.8 ± 0.1	15.5 ± 4.2	0.5 ± 0.2	0.5 ± 0.1	2.4 ± 0.8	1.1 ± 0.4	1.2 ± 0.6	1.2 ± 0.6
^{99m}Tc-B2702p2	0.3 ± 0.1	0.9 ± 0.6	0.8 ± 0.3	2.7 ± 0.3	1.4 ± 0.4	13.4 ± 1.9	0.3 ± 0.2	0.2 ± 0.1	0.9 ± 0.3†	1.3 ± 0.1	0.5 ± 0.2†	0.3 ± 0.1†
^{99m}Tc-B2702p3	0.4 ± 0.1	0.7 ± 0.2	0.9 ± 0.2	4.2 ± 0.6	0.8 ± 0.2	33.1 ± 0.7	0.3 ± 0.1	0.2 ± 0.1	1.3 ± 0.3†	0.6 ± 0.1	0.5 ± 0.1†	0.4 ± 0.1†
^{99m}Tc-B2702p4	0.3 ± 0.1	0.6 ± 0.3	0.6 ± 0.2	4.7 ± 0.9	0.6 ± 0.2	26.2 ± 5.1	0.2 ± 0.1	0.2 ± 0.1	0.9 ± 0.4†	0.6 ± 0.2	0.7 ± 0.4†	0.2 ± 0.1†
^{99m}Tc-B2702p6	0.3 ± 0.0	0.6 ± 0.0	0.7 ± 0.0	5.9 ± 1.0	0.5 ± 0.0	8.2 ± 0.7	0.2 ± 0.0	0.1 ± 0.0	1.1 ± 0.1†	1.5 ± 0.3	0.5 ± 0.1†	0.4 ± 0.2†
^{99m}Tc-B2702p7	0.4 ± 0.0	0.7 ± 0.1	0.9 ± 0.1	8.2 ± 0.4	1.0 ± 0.3	8.0 ± 1.3	0.2 ± 0.0	0.2 ± 0.0	1.3 ± 0.1†	1.9 ± 0.7	0.4 ± 0.2†	0.4 ± 0.2†
^{99m}Tc-B2702p8	0.3 ± 0.1	0.7 ± 0.1	0.9 ± 0.1	6.9 ± 1.6	0.8 ± 0.2	20.6 ± 10.8	0.2 ± 0.1	0.2 ± 0.1	1.2 ± 0.3†	1.6 ± 0.6	0.4 ± 0.1†	0.2 ± 0.1†
^{99m}Tc-B2702p9	0.1 ± 0.0	0.3 ± 0.0	0.4 ± 0.0	2.1 ± 0.1	0.4 ± 0.1	2.2 ± 0.2	0.1 ± 0.0	0.1 ± 0.0	0.4 ± 0.0†	0.4 ± 0.0	0.1 ± 0.0†	0.1 ± 0.0†
^{99m}Tc-B2702P10	0.5 ± 0.3	0.3 ± 0.0	0.4 ± 0.1	2.8 ± 0.5	0.4 ± 0.1	23.6 ± 3.7	0.1 ± 0.0	0.1 ± 0.0	0.4 ± 0.0†	0.3 ± 0.0	0.1 ± 0.0†	0.4 ± 0.2†
^{99m}Tc-B2702p11	1.8 ± 0.1	2.7 ± 0.1	3.6 ± 0.3	10.8 ± 0.6	2.9 ± 0.1	19.2 ± 0.8	1.5 ± 0.3	0.6 ± 0.1	6.7 ± 0.4	14.2 ± 6.9	2.1 ± 0.3	1.9 ± 0.7
^{99m}Tc-B2702p12	0.4 ± 0.1	2.8 ± 0.9	4.2 ± 1.5	5.5 ± 0.6	3.1 ± 0.2	36.9 ± 11.4	0.8 ± 0.1	0.8 ± 0.4	4.4 ± 1.2	8.8 ± 2.8	2.1 ± 0.9	1.4 ± 0.4
^{99m}Tc-B2702p13	1.6 ± 0.3	2.3 ± 0.3	3.3 ± 0.4	8.0 ± 0.6	2.9 ± 0.4	22.7 ± 7.5	0.8 ± 0.3	0.5 ± 0.1	5.9 ± 0.5	11.0 ± 3.2	1.7 ± 0.3	1.8 ± 0.4
^{99m}Tc-B2702p14	2.5 ± 0.7	3.2 ± 0.6	5.7 ± 1.4	12.7 ± 2.4	3.7 ± 1.0	34.6 ± 1.9	0.8 ± 0.1	0.7 ± 0.2	10.7 ± 2.2	15.9 ± 2.6	2.2 ± 0.2	2.2 ± 0.2
^{99m}Tc-B2702p15	4.5 ± 0.3	5.2 ± 0.1	11.2 ± 0.7	18.1 ± 0.7	6.4 ± 0.2	34.0 ± 4.4	1.6 ± 0.7	1.2 ± 0.1	16.4 ± 0.9	6.3 ± 1.1	3.3 ± 0.7	1.9 ± 0.5
^{99m}Tc-B2702p16	0.3 ± 0.0	0.6 ± 0.1	0.9 ± 0.1	3.4 ± 0.4	1.2 ± 0.1	98.9 ± 18.1	0.4 ± 0.1	0.2 ± 0.0	1.0 ± 0.1†	1.7 ± 0.2	0.4 ± 0.0†	0.4 ± 0.2†
^{99m}Tc-B2702p17	0.4 ± 0.1	0.6 ± 0.2	1.2 ± 0.5	3.5 ± 1.2	1.6 ± 0.7	85.3 ± 25.7	0.3 ± 0.1	0.3 ± 0.2	1.3 ± 0.4†	2.8 ± 0.4	0.4 ± 0.1†	0.2 ± 0.1†
^{99m}Tc-B2702p18	0.5 ± 0.1	2.5 ± 0.4	3.2 ± 0.5	6.3 ± 1.5	2.3 ± 0.7	63.9 ± 17.2	1.2 ± 0.5	0.7 ± 0.0	5.9 ± 1.0	18.8 ± 2.7	2.0 ± 0.2*	1.0 ± 0.1†
^{99m}Tc-B2702p19	0.5 ± 0.1	0.9 ± 0.3	1.3 ± 0.2	5.5 ± 0.5	1.5 ± 0.1	15.2 ± 6.0	0.2 ± 0.0	0.3 ± 0.0	2.0 ± 0.5†	1.9 ± 1.5	0.7 ± 0.1†	1.1 ± 0.5
^{99m}Tc-B2702p20	0.6 ± 0.2	1.4 ± 0.4	1.2 ± 0.3	6.1 ± 1.1	1.0 ± 0.4	11.1 ± 2.0	0.2 ± 0.1	0.2 ± 0.1	2.2 ± 0.6†	0.5 ± 0.2	0.9 ± 0.1†	1.2 ± 0.8

Data are mean ± SE %ID/g. *$P < 0.05$ vs. right carotid. †$P < 0.05$ vs. ^{99m}Tc-B2702p.

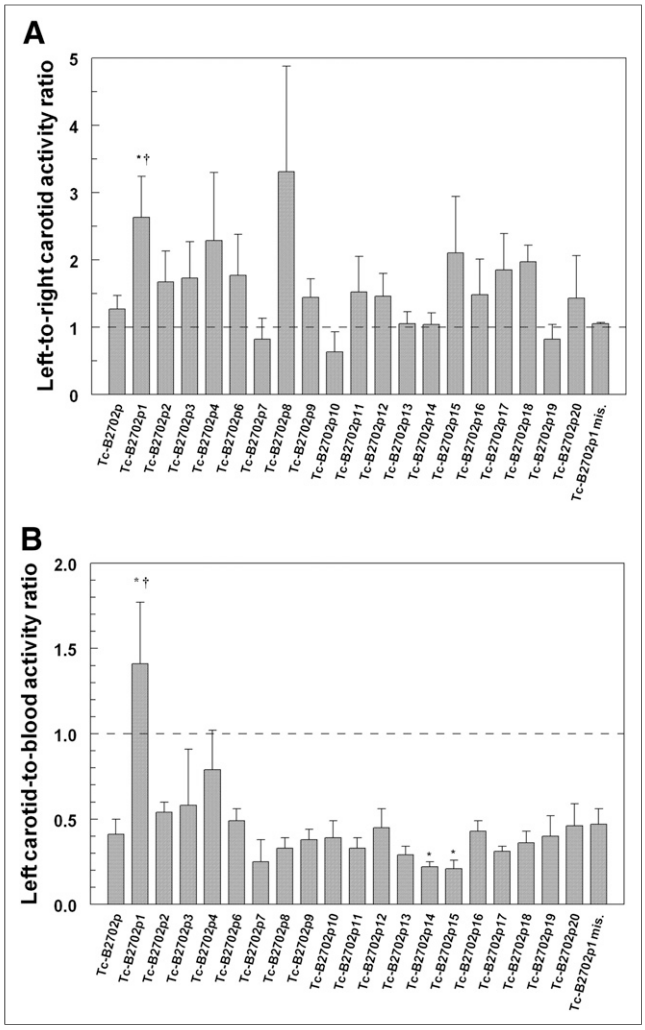

FIGURE 2. Left-to-right carotid (A) and left carotid-to-blood (B) activity ratios of ^{99m}Tc-labeled peptidic sequences as determined by γ-well counting at 180 min after intravenous tracer injection. mis. = mismatch. *$P < 0.05$ vs. ^{99m}Tc-B2702p. †$P < 0.05$ vs. ^{99m}Tc-B2702p1 mismatch.

tive VCAM-1 and Mac-2 immunostaining was observed in atherosclerotic lesions developing at the site of left carotid artery ligation but not in contralateral, right, carotid arteries or in vessels from sham-operated animals. In addition, immunohistochemical staining indicated no signs of postsurgery skin inflammation at the time of tracer injection, because the 3-wk interval between surgery and image acquisition had allowed for complete healing of the incision site.

Biodistribution Studies

As indicated in Table 1, all peptidic sequences were successfully radiolabeled with a radiochemical purity of more than 88% with the exception of B2702p5 (~50%), which was therefore not further considered for evaluation. All radiotracers displayed good urinary stability with the exception of B2702p7 and B2702p16. The 180-min biodistribution of all radiotracers is presented in Table 2. The kidneys represented the preferential route of excretion for all tracers except for ^{99m}Tc-B2702p1 mismatch, ^{99m}Tc-B2702p7, and ^{99m}Tc-B2702p9, for which the hepatobiliary route was equally involved. Significant thyroid uptake likely indicative of radiolabeling instability after in vivo injection was observed for ^{99m}Tc-B2702p, ^{99m}Tc-B2702p11, ^{99m}Tc-B2702p12, ^{99m}Tc-B2702p13, ^{99m}Tc-B2702p14, ^{99m}Tc-B2702p15, and ^{99m}Tc-B2702p18. ^{99m}Tc-B2702p1 and ^{99m}Tc-B2702p18 left carotid activity was significantly higher than the activity observed in the right carotid artery. Shown in Figure 2 are the left-to-right carotid activity ratios and left carotid-to-blood activity ratios for all radiotracers. ^{99m}Tc-B2702p1 left-to-right carotid and left carotid-to-blood activity ratios at 180 min (2.6 ± 0.6 and 1.4 ± 0.4, respectively) were significantly

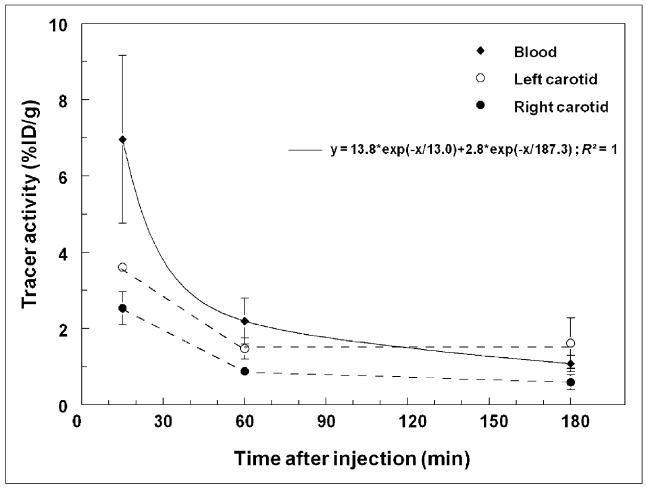

FIGURE 3. Time–activity curves of ^{99m}Tc-B2702p1 in blood and left and right carotid arteries at 15, 60, and 180 min after intravenous injection of tracer.

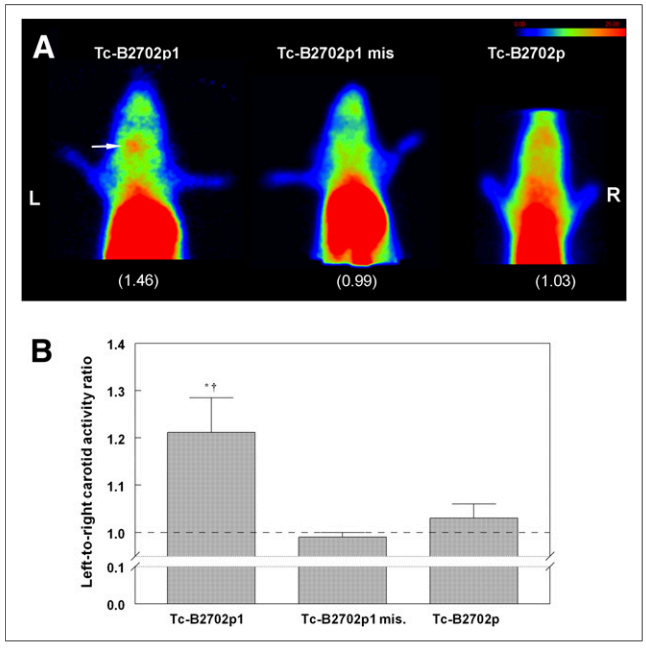

FIGURE 4. (A) Representative planar images of ApoE$^{-/-}$ mouse with left carotid artery ligation at 180 min after injection of ^{99m}Tc-B2702p1, ^{99m}Tc-B2702p1 mismatch, and ^{99m}Tc-B2702p; corresponding left-to-right carotid tracer activity ratios are indicated in parentheses. (B) ^{99m}Tc-B2702p1, ^{99m}Tc-B2702p1 mismatch, and ^{99m}Tc-B2702p left-to-right carotid activity ratios from in vivo planar image quantification. *$P < 0.05$ vs. ^{99m}Tc-B2702p. †$P < 0.05$ vs. ^{99m}Tc-B2702p1 mismatch. mis = mismatch.

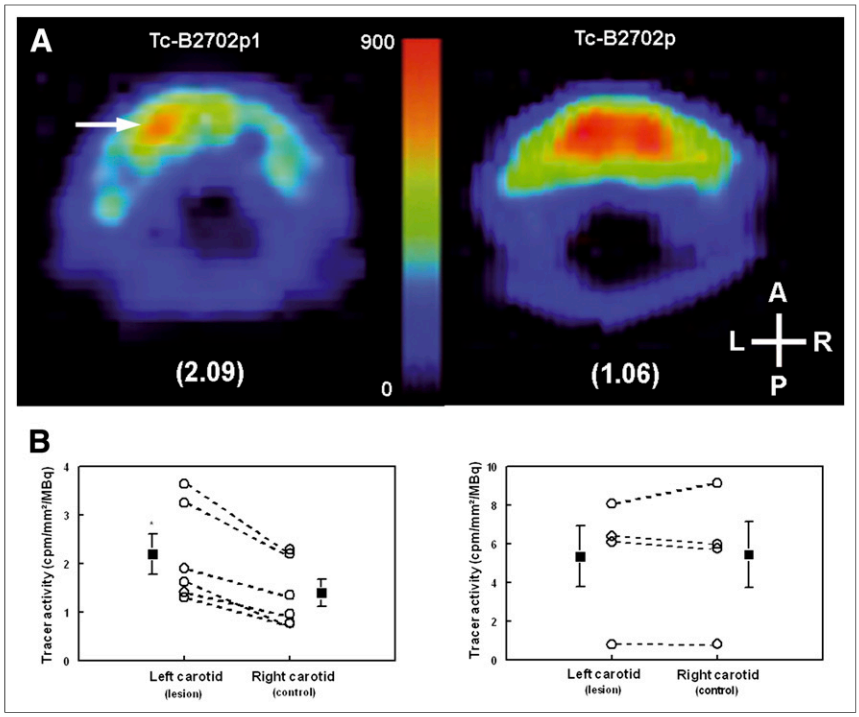

FIGURE 5. (A) Representative pinhole SPECT image of ^{99m}Tc-B2702p1 and ^{99m}Tc-B2702p activity at level of atherosclerotic lesion developing at site of left carotid artery ligation in ApoE$^{-/-}$ mouse. Corresponding left-to-right carotid tracer activity ratios are indicated in parentheses. (B) Left and right ^{99m}Tc-B2702p1 (left) and ^{99m}Tc-B2702p (right) carotid activities from in vivo pinhole SPECT image quantification. *$P < 0.05$ vs. right carotid tracer activity.

higher than those of ^{99m}Tc-B2702p (1.3 ± 0.2 and 0.4 ± 0.1, respectively) and ^{99m}Tc-B2702p1 mismatch (1.1 ± 0.0 and 0.5 ± 0.1, respectively). In addition, ^{99m}Tc-B2702p1 was the only tracer with a left carotid-to-blood activity ratio greater than 1. Finally, the blood kinetics of ^{99m}Tc-B2702p1 were best fitted using a biexponential fit with half-lives of 13 min and 187 min (Fig. 3). Also shown in Figure 3 is the comparison between blood activity, left carotid activity, and right carotid activity, indicating that 180 min after injection represented the optimal time for in vivo imaging.

In Vivo Imaging

Representative in vivo planar images acquired between 150 and 180 min after the injection of ^{99m}Tc-B2702p1, ^{99m}Tc-B2702p1 mismatch, and ^{99m}Tc-B2702p are displayed in Figure 4A. The results indicated that the atherosclerotic lesion expressing VCAM-1 and developing on the left carotid artery after vessel ligation was readily visualized after the injection of ^{99m}Tc-B2702p1 but not after ^{99m}Tc-B2702p1 mismatch or ^{99m}Tc-B2702p. Results from in vivo planar image quantification are shown in Figure 4B. The ^{99m}Tc-B2702p1 left-to-right carotid activity ratio (1.2 ± 0.1) was significantly higher than those of ^{99m}Tc-B2702p (1.0 ± 0.0) and ^{99m}Tc-B2702p1 mismatch (1.0 ± 0.0). These results were further confirmed after in vivo pinhole SPECT imaging of ^{99m}Tc-B2702p1 left carotid lesion uptake. As shown in Figure 5, ^{99m}Tc-B2702p1 left carotid activity was higher than activity observed in the contralateral vessel in all animals (mean values, 2.2 ± 0.4 and 1.4 ± 0.3 cpm/mm^2/MBq, respectively, $P < 0.01$), resulting in a left-to-right carotid activity ratio of 1.6 ± 0.1 after injection of ^{99m}Tc-B2702p1.

In Vitro Experiments

The results from fluorescence polarization experiments are presented in Figure 6. An increasing anisotropy value was observed in the presence of increasing VCAM-1 concentrations, and a plateau was reached. A K_d value of 15×10^{-6} M for the interaction between VCAM-1 and [F]-B2702p1 was determined assuming a one-to-one interaction ("Materials and Methods"). This value was approximately 40-fold lower than that observed in the presence of bovine serum albumin (5.95×10^{-4} M).

DISCUSSION

^{99m}Tc-B2702p has been previously validated as a tracer of VCAM-1 expression in a Watanabe heritable hyperlipidemic rabbit model of atherosclerosis (*15*). However, the suboptimal blood kinetics of the tracer prevented in vivo image acquisition. In the present study, we hypothesized that the in vivo kinetics of ^{99m}Tc-B2702p might be improved by discrete modifications of the amino acid sequence of the peptide, thereby allowing the in vivo imaging of VCAM-1 expression. Derived peptides were therefore initially generated following an alanine scan methodology consisting of the systematic replacement of the original residues with an alanine in each position of the peptide. Additional modifications were also performed by inverting 2 residues before reiterating the alanine scan methodology on the premodified peptide (Table 1). The alanine scan strategy has been previously used to investigate the structure–activity relationship of peptidic receptor antagonists (*17*). Alanine scan modifications have been described as either decreasing, having no effect on, or possibly increasing the potency and metabolic stability of the peptide being modified (*17–19*).

Twenty peptides were therefore generated from the original B2702p sequence and labeled with ^{99m}Tc using the Isolink method for biologic evaluation on an ApoE$^{-/-}$ mouse model of atherosclerosis. Briefly, a focal atherosclerotic lesion was induced in hypercholesterolemic ApoE$^{-/-}$ animals by left carotid artery ligation. This model was previously validated as suitable for the experimental evaluation of potential radiotracers of atherosclerotic plaques (*22*). In the present study, we verified that VCAM-1 expression occurred at the site of plaque development but not in the contralateral vessel as illustrated by immunohistology experiments. The overexpression of VCAM-1 was concomitant with the presence of macrophages and thereby indicative of the occurrence of an inflammatory process similar to that observed in vulnerable lesions.

The results from biodistribution studies indicated that the highest left-to-right carotid and left carotid-to-blood activity ratios were obtained after the injection of ^{99m}Tc-B2702p1. In addition, ^{99m}Tc-B2702p1 was the only derivative with a left carotid-to-blood activity ratio greater than 1, suggesting that the tracer target-to-background ratio would be suitable for the in vivo imaging of VCAM-1 expression. In vivo planar imaging studies confirmed this hypothesis. Indeed, the atherosclerotic lesion developing at

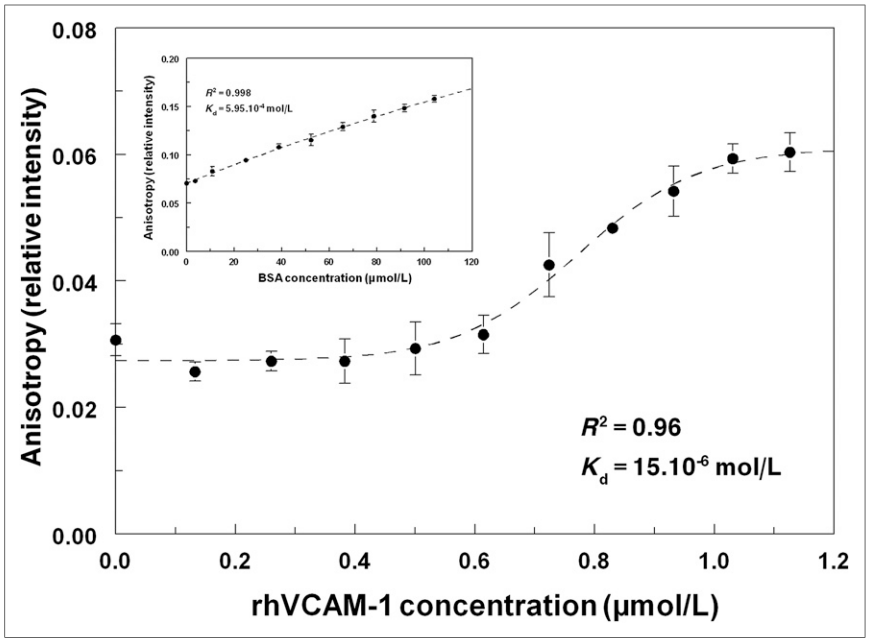

FIGURE 6. Anisotropy values from [F]-B2702p1 in presence of increasing concentrations of recombinant human VCAM-1. Results from control experiments performed in absence of VCAM-1 and in presence of nonspecific target bovine serum albumin are shown in inset.

the site of left carotid artery ligation was readily identified after injection of ^{99m}Tc-B2702p1. ^{99m}Tc-B2702p injection resulted in significant thyroid activity as indicated by the biodistribution data presented in Table 2, which might indicate suboptimal in vivo tracer stability whereas thyroid activity remained low after ^{99m}Tc-B2702p1 injection, in accordance with good in vivo tracer stability. However, high ^{99m}Tc-B2702p circulating tracer activity (Table 2) and small thyroid dimensions likely precluded thyroid visualization on planar images whereas low ^{99m}Tc-B2702p1 circulating and thyroid activities allowed the imaging of ^{99m}Tc-B2702p1–specific uptake in atherosclerotic lesions. High-resolution tomographic imaging experiments yielded results similar to those observed using planar imaging, with a systematically higher tracer activity in the atherosclerotic lesion located on the left carotid artery than in the contralateral vessel, leading to a mean left-to-right carotid tracer activity ratio of 1.6 ± 0.1. The specificity of ^{99m}Tc-B2702p1 binding to VCAM-1 in vivo was demonstrated by the fact that atherosclerotic plaque could not be imaged after the injection of ^{99m}Tc-B2702p1 mismatch, the peptidic sequence that consisted of similar amino acids in a random peptidic sequence.

The affinity of the B2702p1 peptidic sequence for VCAM-1 was determined with fluorescence polarization using a methodology similar to that previously used to evaluate the K_d value corresponding to the interaction between B2702p and VCAM-1 (*15*). The K_d value for the interaction between B2702p1 and VCAM-1 was approximately 15 μmol/L, a value about 50-fold higher than that for B2702, consistent with the observation that a decrease in ligand affinity frequently occurs with the alanine scan methodology (*17*). Several peptidic VCAM-1 ligands were recently described. In vitro phage display allowed the selection of the multimodal viral nanoparticle (*23*), whereas in vivo phage display led to the discovery of VCAM-1 internalizing nanoparticle 28 (VINP-28), a linear sequence that allowed the in vivo imaging of atherosclerotic lesions using MR imaging and optical imaging (*24*). More recently, a tetrameric peptide of nanomolar affinity for VCAM-1 and consisting of 4 VINP-28 sequences allowed the nuclear imaging of ApoE$^{-/-}$ mouse atherosclerotic lesions after radiolabeling with ^{18}F (*25*). In addition, the recently described R832 short peptidic sequence was obtained using the in vitro phage display methodology as well. The peptide displayed a micromolar affinity for VCAM-1 and allowed the in vivo detection of VCAM-1 expression after conjugation to gadolinium-DOTA and MR imaging (*26*). Taken altogether, the results from these studies suggest that a wide range of affinities might be suitable for the noninvasive imaging of molecular targets.

The affinity of the peptidic sequence B2702p1 described in the present study for VCAM-1 is similar to that of R832. Importantly, the discrete amino acid modifications that led to the B2702p1 peptide from the original B2702p sequence led to a decreased circulating activity for ^{99m}Tc-B2702p1 when compared with ^{99m}Tc-B2702p. Indeed, blood activity was more than 6-fold lower for ^{99m}Tc-B2702p1 than for ^{99m}Tc-B2702p, leading to a target-to-background ratio suitable for in vivo imaging. On the other hand, the elevated circulating blood activity of ^{99m}Tc-B2702p together with a suboptimal stability of the tracer after in vivo injection as illustrated by the significant thyroid activity prevented the successful acquisition of in vivo images of VCAM-1 expression.

CONCLUSION

B2702p1 was selected among 20 alanine scan derivatives of the previously described peptidic sequence B2702p as the tracer allowing the in vivo imaging of VCAM-1 expression in a murine model of atherosclerosis after radiolabeling with ^{99m}Tc. Further clinical studies are needed to determine the potential of the tracer for the detection of vulnerable atherosclerosis in patients.

DISCLOSURE

The costs of publication of this article were defrayed in part by the payment of page charges. Therefore, and solely to indicate this fact, this article is hereby marked "advertisement" in accordance with 18 USC section 1734. This research was supported by a grant from the Agence Nationale de la Recherche (ANR-PLAQUIMAG 2010-13 program), the Agence Nationale pour la Recherche et la Technologie (ANRT-CIFRE), and ERAS Labo. No other potential conflict of interest relevant to this article was reported.

ACKNOWLEDGMENTS

We acknowledge the Anatomopathology Department and Nuclear Medicine Department staff (CHU, Grenoble, France) for assistance with histology and radiolabeling and René Bontron for assistance with animals.

REFERENCES

1. Roger VL, Go AS, Lloyd-Jones DM, et al. Heart disease and stroke statistics: 2011 update—a report from the American Heart Association. *Circulation.* 2011;123:e18–e209.

2. Naghavi M, Falk E, Hecht HS, et al. From vulnerable plaque to vulnerable patient—part III: executive summary of the Screening for Heart Attack Prevention and Education (SHAPE) Task Force report. *Am J Cardiol.* 2006;98: 2H–15H.
3. Naghavi M, Libby P, Falk E, et al. From vulnerable plaque to vulnerable patient: a call for new definitions and risk assessment strategies—part II. *Circulation.* 2003;108:1772–1778.
4. Naghavi M, Libby P, Falk E, et al. From vulnerable plaque to vulnerable patient: a call for new definitions and risk assessment strategies—part I. *Circulation.* 2003;108:1664–1672.
5. Sadeghi MM, Glover DK, Lanza GM, Fayad ZA, Johnson LL. Imaging atherosclerosis and vulnerable plaque. *J Nucl Med.* 2010;51(suppl 1):51S–65S.
6. Riou LM, Broisat A, Dimastromatteo J, Pons G, Fagret D, Ghezzi C. Pre-clinical and clinical evaluation of nuclear tracers for the molecular imaging of vulnerable atherosclerosis: an overview. *Curr Med Chem.* 2009;16:1499–1511.
7. Iiyama K, Hajra L, Iiyama M, et al. Pattern of vascular cell adhesion molecule-1 and intercellular adhesion molecule-1 expression in rabbit and mouse atherosclerotic lesions and at sites predisposed to lesion formation. *Circ Res.* 1999;85: 199–207.
8. Ley K, Huo Y. VCAM-1 is critical in atherosclerosis. *J Clin Invest.* 2001;107: 1209–1210.
9. Cybulsky MI, Liyama K, Li H, et al. A major role for VCAM-1 but not ICAM-1, in early atherosclerosis. *J Clin Invest.* 2001;107:1255–1262.
10. O'Brien KD, Allen MD, McDonald TO, et al. Vascular cell adhesion molecule-1 is expressed in human coronary atherosclerotic plaques. *J Clin Invest.* 1993; 92:945–951.
11. O'Brien KD, McDonald TO, Chait A, Allen MD, Alpers CE. Neovascular expression of E-selectin, intercellular adhesion molecule-1 and vascular adhesion molecule-1 in human atherosclerosis and their relation to intimal leucocyte content. *Circulation.* 1996;93:672–682.
12. Ramos CL, Huo Y, Jung U, et al. Direct demonstration of P-selectin- and VCAM-1-dependent mononuclear cell rolling in early atherosclerotic lesions of apolipoprotein E-deficient mice. *Circ Res.* 1999;84:1237–1244.
13. Davies MJ, Gordon JL, Gearing AJ, et al. The expression of the adhesion molecules ICAM-1, VCAM-1, PECAM, and E-selectin in human atherosclerosis. *J Pathol.* 1993;171:223–229.
14. Orr AW, Hastings NE, Blackman BR, Wamhoff BR. Complex regulation and function of the inflammatory smooth muscle cell phenotype in atherosclerosis. *J Vasc Res.* 2010;47:168–180.
15. Broisat A, Riou LM, Ardisson V, et al. Molecular imaging of vascular cell adhesion molecule-1 expression in experimental atherosclerotic plaques with radiolabelled B2702-p. *Eur J Nucl Med Mol Imaging.* 2007;34:830–840.
16. Ling X, Tamaki T, Xiao Y, et al. An immunosuppressive and anti-inflammatory HLA class I derived peptides binds vascular cell adhesion molecule-1. *Transplantation.* 2000;70:662–667.
17. Quartara L, Ricci R, Meini S, et al. Ala scan analogues of HOE 140: synthesis and biological activities. *Eur J Med Chem.* 2000;35:1001–1010.
18. Marrakchi N, Mabrouk K, Regaya I, et al. Lebetin peptides: potent platelet aggregation inhibitors. *Haemostasis.* 2001;31:207–210.
19. Van Craenenbroeck M, Gregoire F, De Neef P, Robberecht P, Perret J. Ala-scan of ghrelin (1-14): interaction with the recombinant human ghrelin receptor. *Peptides.* 2004;25:959–965.
20. Sörme P, Kahl-Knutsson B, Huflejt M, Nilsson UJ, Leffler H. Fluorescence polarization as an analytical tool to evaluate galectin-ligand interactions. *Anal Biochem.* 2004;334:36–47.
21. Broisat A, Toczek J, Mesnier N, et al. Assessing low levels of mechanical stress in aortic atherosclerotic lesions from apolipoprotein E−/− mice. *Arterioscler Thromb Vasc Biol.* 2011;31:1007–1010.
22. Schäfers M, Riemann B, Kopka K, et al. Scintigraphic imaging of matrix metalloproteinase activity in the arterial wall in vivo. *Circulation.* 2004;109:2554–2559.
23. Kelly KA, Allport JR, Tsourkas A, Shinde-Patil VR, Josephson L, Weissleder R. Detection of vascular adhesion molecule-1 expression using a novel multimodal nanoparticle. *Circ Res.* 2005;96:327–336.
24. Nahrendorf M, Jaffer FA, Kelly KA, et al. Noninvasive vascular cell adhesion molecule-1 imaging identifies inflammatory activation of cells in atherosclerosis. *Circulation.* 2006;114:1504–1511.
25. Nahrendorf M, Keliher E, Panizzi P, et al. ^{18}F-4V for PET-CT imaging of VCAM-1 expression in inflammatory atherosclerosis. *JACC Cardiovasc Imaging.* 2009;2:1213–1222.
26. Burtea C, Laurent S, Port M, et al. Magnetic resonance molecular imaging of vascular cell adhesion molecule-1 expression in inflammatory lesions using a peptide-vectorized paramagnetic imaging probe. *J Med Chem.* 2009;52:4725–4742.